Fibonacci Laws of Planetary Motion and a Unified Theory of Earth's Precession Cycles

D. van Sonsbeek*

Independent Researcher, Den Dolder, The Netherlands

February 19, 2026

Abstract

Three major frameworks in planetary science — Kepler's orbital geometry, Milankovitch climate theory, and Laplace–Lagrange secular perturbation theory — describe planetary motion with high precision, yet no unifying principle connects precession timescales, orbital amplitudes, and the collective structure of the solar system. We present a geometric model in which two counter-rotating reference points, with periods in the Fibonacci ratio 13:3, generate a 333,888-year master cycle from which all major precession periods emerge as integer Fibonacci divisions. From this single timescale we identify six structural laws connecting the orbital inclinations and eccentricities of all eight planets through Fibonacci numbers: a cycle hierarchy generating all precession periods (Law 1), paired individual-constant and collective-balance constraints on inclinations (Laws 2–3) and eccentricities (Laws 4–5), and a closed Saturn–Jupiter–Earth beat-frequency resonance (Law 6). All six laws require zero free parameters beyond the master cycle itself. Twelve statistical tests yield Fisher's combined $p \leq 7.1 \times 10^{-14}$; the TRAPPIST-1 system independently exhibits the same Fibonacci structure. The framework produces testable consequences for Earth, including a unified obliquity formula, an eccentricity mechanism driven by perihelion precession and coupled to Saturn, a proposed resolution of the 100,000-year problem through inclination precession, and a time-varying Mercury perihelion anomaly. The model generates 17 specific predictions; BepiColombo (science operations from 2027) provides a near-term discriminating test. The model uses 6 adjustable parameters; all data, formulas, and a 3D simulation are publicly available.

Keywords: celestial mechanics, precession, obliquity, eccentricity, Milankovitch cycles, orbital dynamics, Fibonacci sequence, invariable plane, reference frame effects, BepiColombo, Mercury perihelion, angular momentum deficit, KAM theory

1. Introduction

1.1 The Missing Link

Modern astronomy describes planetary orbits with extraordinary precision, yet three major frameworks operate in isolation. Kepler's laws describe orbital geometry. Milankovitch theory describes Earth's climate cycles through eccentricity, obliquity, and precession. Laplace–Lagrange secular theory describes long-term orbital perturbations and angular momentum exchange. No framework connects the *timescales* of precession, the *amplitudes* of orbital inclinations and eccentricities, and the *collective structure* of the solar system within a single mathematical description.

This disconnection leaves fundamental questions unanswered. Why does Earth's obliquity oscillate at ~41,000 years? Why does eccentricity vary quasi-periodically? Why do Fibonacci ratios appear in planetary period ratios (Pletser, 2019; Aschwanden, 2018)? Each question has partial answers within its own framework, but no unifying principle connects them.

1.2 Open Questions

Three long-standing problems motivate this work:

1. **The 100,000-year problem**: Geological records show a dominant ~100,000-year glacial cycle, but Milankovitch eccentricity provides only ~0.2% insolation change — too weak without amplification mechanisms (Hays et al., 1976; Muller & MacDonald, 1997a). The theoretically dominant ~400,000-year eccentricity cycle is largely absent from climate records. This remains unsolved: Barker et al. (2025) continue to debate the distinct roles of precession, obliquity, and eccentricity, while the Mid-Pleistocene Transition is described as "one of paleoclimatology's great unsolved puzzles."
2. **No unified precession framework**: Axial precession (luni-solar torque), apsidal precession (planetary perturbations), and obliquity variation (secular perturbations) share gravitational origins but are modeled independently (Capitaine et al., 2003; Laskar, 1993; Berger, 1988).
3. **No single-formula predictions**: Current models rely on polynomial fits to numerical integrations, valid over limited time ranges. Vondrák et al. (2011) extended IAU 2006 precession to ±200,000 years — the state of the art. No closed-form solution exists for the gravitational n-body problem.

1.3 The Holistic Universe Model

The starting point is an empirical observation: two of Earth's precession motions — axial and inclination — rotate in *opposite directions*, and their periods relate as a Fibonacci ratio (13:3). The Holistic Universe Model explores the consequences of this ratio within a geocentric 3D software simulation built from 6 adjustable parameters that reproduces all major solar system movements: invariable plane orientation, inclination and perihelion precession, eccentricity cycles, obliquity, and planetary orbits.

The methodology is empirical-first: orbital parameters were measured from the simulation, exported to independent analysis tools, and only then were analytical formulas and structural laws identified from the numerical output. Two categories of results emerged. First, closed-form formulas for obliquity, eccentricity, precession rates, and day/year lengths at any epoch (the 273-term predictive system, Section 11). Second, six Fibonacci Laws connecting all eight planets through Fibonacci numbers and a single timescale. The simulation serves as both discovery tool and independent test bed: established results such as the invariable plane orientation of Souami & Souchay (2012) can be verified within the same framework. The simulation is publicly available[1] and documented in full[2].

The model does not claim to replace n-body gravitational theory. Rather, it proposes a geometric framework that captures regularities in the solar system's dynamics not immediately visible in numerical integrations.

1.4 This Paper's Contribution

We present six Fibonacci Laws of planetary motion derived from a geometric model of the solar system. The paper is organized in three parts:

- **Part I** (Sections 2–7): The Fibonacci structure — the model, the six laws, statistical significance, and exoplanet evidence
- **Part II** (Sections 8–10): Consequences for Earth — observable Earth dynamics, the 100,000-year climate problem, and Mercury's perihelion as a reference frame effect
- **Part III** (Sections 11–15): Predictions and validation — predictive formulas, calibration transparency, 17 testable predictions, and discussion

Part I: The Fibonacci Structure

2. The Model: Two Counter-Rotating Reference Points

2.1 Foundation

The model is built on two mathematical constructs — not physical objects, but reference points that parameterize known precession phenomena:

Earth-Wobble-Center: A point near Earth (~213,000 km, or 0.001431 AU), around which Earth traces its axial precession circle clockwise (as seen from the north ecliptic pole). Mean orbital period: 25,683.69 years. This represents the luni-solar precession.

Perihelion-of-Earth: The direction of Earth's closest approach to the Sun, modeled as a point at distance 0.015321 AU from the Sun, orbiting counter-clockwise. Mean orbital period: 111,296 years. This represents the planetary precession.

The model recasts these as two counter-rotating circular motions within a single geometric framework (Fig. 1).

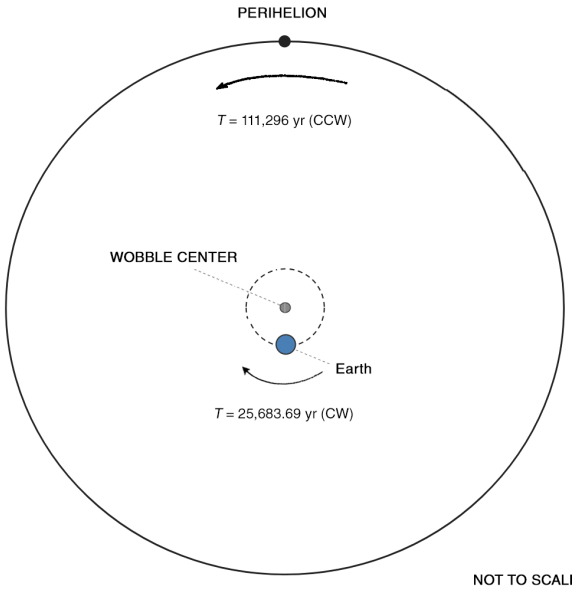

Figure 1: Schematic of the two counter-rotating reference points. Earth orbits the Earth-Wobble-Center clockwise (CW) with period T = 25,683.69 years, while the Perihelion-of-Earth orbits counter-clockwise (CCW) around the Sun with period T = 111,296 years. The 13:3 ratio produces the 333,888-year Holistic-Year. Not to scale.

2.2 The Fibonacci Ratio and KAM Theory

The ratio of the two fundamental periods is:

$$\frac{T_{\text{incl}}}{T_{\text{axial}}} = \frac{111{,}296}{25{,}683.69} = 4.333\ldots = \frac{13}{3} \tag{1}$$

Both 3 and 13 are Fibonacci numbers (F_4 and F_7). This has theoretical grounding in the Kolmogorov–Arnold–Moser (KAM) theorem, which proves that orbital systems with "most irrational" frequency ratios are maximally stable against perturbation (Morbidelli & Giorgilli, 1995). The golden ratio $\varphi \approx 1.618$, to which successive Fibonacci ratios converge, is the most irrational number in a precise mathematical sense. Greene (1979) showed computationally that the golden-ratio torus is the last to break under perturbation. Pletser (2019) demonstrated that orbital period ratios preferentially cluster near Fibonacci fractions (~60% vs ~40% for non-Fibonacci), and Aschwanden (2018) found Fibonacci fractions in 73% of 932 exoplanet pairs. The 13:3 ratio thus reflects a maximally stable configuration predicted by dynamical systems theory.

2.3 The Holistic-Year and Derived Cycles

The 13:3 ratio produces a master cycle:

$$T_{\text{Holistic}} = 13\times25{,}683.69 = 3\times111{,}296 = 333{,}888 \text{ years} \tag{2}$$

All subsidiary cycles emerge as integer divisions of the Holistic-Year (Table 1).

[1] https://3d.holisticuniverse.com
[2] https://holisticuniverse.com

Table 1: Derived cycles from the Holistic-Year (Law 1)

Cycle	Divisor	Duration (yr)	Fibonacci?
Holistic-Year	1	333,888	$F_1 = 1$
Incl. precession (ICRF)	3	111,296	$F_4 = 3$
Incl. precession (ecliptic)	5	66,778	$F_5 = 5$
Obliquity cycle	8	41,736	$F_6 = 8$
Axial precession	13	25,684	$F_7 = 13$
Perihelion precession	16	20,868	$13 + 3 = 16$

The perihelion precession period emerges from the meeting frequency of the two counter-rotating motions:

$$\frac{1}{T_{\text{perihelion}}} = \frac{1}{T_{\text{axial}}} + \frac{1}{T_{\text{incl}}} = \frac{1}{25{,}684} + \frac{1}{111{,}296} = \frac{1}{20{,}868} \quad (3)$$

The frequencies add (rather than subtract) because the motions are in opposite directions.

2.4 The Balanced Year (Epoch Anchor)

The model uses a reference epoch called the Balanced Year, calculated from the last perihelion–solstice alignment:

$$T_{\text{balanced}} = 1246\,\text{AD} - 14.5 \times 20{,}868 = -301{,}340 \quad (4)$$

At this epoch (301,340 BC), the axial tilt effect and inclination tilt effect are in exact opposition, producing obliquity at its mean value (~23.41°). The value is not arbitrary: within the 333,888-year cycle, the observed inclination trend (currently decreasing) and the observed obliquity trend (currently decreasing) must be simultaneously reproduced. Only a narrow range of phase offsets achieves this, and $14.5 \times 20{,}868$ emerged as the only configuration consistent with all observational constraints — the current rates of change, the J2000 values, and the known oscillation ranges. This serves as the phase-zero reference for all cycle calculations, analogous to how J2000 serves as the standard astronomical epoch.

3. Law 1: Fibonacci Cycle Hierarchy

Dividing the Holistic-Year $H = 333{,}888$ by successive Fibonacci numbers produces every major precession period of the solar system.

The resulting periods (Table 1) obey a beat-frequency rule inherited from the Fibonacci recurrence $F_n + F_{n+1} = F_{n+2}$:

$$\frac{1}{H/F_n} + \frac{1}{H/F_{n+1}} = \frac{1}{H/F_{n+2}} \quad (5)$$

Any two consecutive Fibonacci periods combine to produce the next. The entire hierarchy is generated by the interaction of just two physical periods — the axial precession ($H/13$) and the inclination precession ($H/3$) — through successive beat frequencies. Law 6 (Section 6) reveals the physical mechanism behind this hierarchy.

4. Laws 2–3: Inclination Structure

4.1 Mass-Weighted Variables and AMD

The planetary data reveals deeper structure when expressed in mass-weighted variables:

- Mass-weighted eccentricity: $\xi = e \times \sqrt{m}$
- Mass-weighted inclination amplitude: $\eta = \text{amplitude} \times \sqrt{m}$

The square root of mass is not arbitrary — it is the unique exponent arising from the Angular Momentum Deficit (AMD) decomposition, the key conserved quantity governing long-term orbital stability (Laskar, 1997). A numerical scan over all mass exponents from 0 to 1 supports this: the products $d \times \eta$ across all eight planets converge to a single value only at exponent 0.50, with a relative spread of 0.11%. No other exponent achieves a spread below 28%.

4.2 The Invariable Plane

The invariable plane — perpendicular to the solar system's total angular momentum vector, dominated by Jupiter (~60%) and Saturn (~25%) — serves as the model's spatial reference. Unlike the ecliptic, which itself precesses, the invariable plane is fixed in inertial space. When measured against it, all planetary inclinations show smooth, predictable oscillations (Table 2).

Table 2: Planetary inclination oscillations relative to the invariable plane

Planet	J2000 (°)	Mean (°)	Ampl. (°)	Period (yr)
Mercury	6.347	6.728	±0.386	242,828
Venus	2.155	2.208	±0.062	667,776
Earth	1.579	1.482	±0.634	111,296
Mars	1.631	2.653	±1.163	77,051
Jupiter	0.322	0.329	±0.021	66,778
Saturn	0.926	0.932	±0.065	41,736
Uranus	0.995	1.001	±0.024	111,296
Neptune	0.735	0.722	±0.014	667,776

Determining which Fibonacci d-value and phase angle belongs to each planet requires searching over millions of possible assignments. The most likely configuration — the only mirror-symmetric solution among 755 valid candidates, calibrated against JPL WebGeocalc data — predicts that Earth and Uranus share the same period (111,296 yr), Venus and Neptune share 667,776 yr ($= 2H$), Jupiter's period equals the ecliptic precession, and Saturn's equals the obliquity cycle — suggesting these planets drive the corresponding Earth cycles.

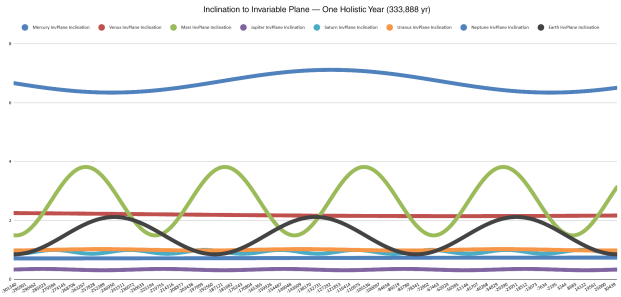

Figure 2: Inclination oscillations of all eight planets relative to the invariable plane over one Holistic Year ($H = 333{,}888$ yr). Mars has the largest amplitude and shortest period (~4.3 cycles); Earth and Uranus share the same period (3 cycles), as do Venus and Neptune (~0.5 cycles). Saturn completes 8 full cycles, linking its period ($H/8$) to the obliquity cycle.

4.3 Law 2: The Inclination Constant

Each planet's mass-weighted inclination amplitude, multiplied by a Fibonacci quantum number, equals the same universal constant.

Defining η = amplitude $\times \sqrt{m}$, every planet satisfies:

$$d \times \eta = \psi \tag{6}$$

where d is a Fibonacci integer specific to each planet. The constant ψ is expressed purely in terms of Fibonacci numbers and H:

$$\psi = \frac{F_5 \times F_8^2}{2H} = \frac{5 \times 21^2}{2 \times 333{,}888} = \frac{2205}{667{,}776} = 3.302 \times 10^{-3} \tag{7}$$

The Fibonacci indices (5, 8) coincide with the period denominators of Jupiter ($H/5$) and Saturn ($H/8$), and the denominator factor $2 = F_3$ coincides with Earth's ($H/3$). Why these specific Fibonacci numbers appear in this combination remains an open question; empirically, the three planets whose periods define them — Earth, Jupiter, and Saturn — are also the three whose mass-weighted inclination amplitudes satisfy the Fibonacci addition rule $3\,\eta_E + 5\,\eta_J = 8\,\eta_S$ to 0.69%, anchoring the entire structure.

With zero free parameters, the model predicts inclination amplitudes for all eight planets (Table 3).

Table 3: Law 2: Inclination constant predictions

Planet	d	Fibonacci	Predicted amp	Mirror pair
Mercury	21	F_8	0.386°	↔ Uranus
Venus	34	F_9	0.062°	↔ Neptune
Earth	3	F_4	0.635°	↔ Saturn
Mars	5	F_5	1.163°	↔ Jupiter
Jupiter	5	F_5	0.021°	↔ Mars
Saturn	3	F_4	0.065°	↔ Earth
Uranus	21	F_8	0.024°	↔ Mercury
Neptune	34	F_9	0.014°	↔ Venus

Maximum deviation from observed amplitudes (Table 2): 0.16% (Earth). All eight predicted ranges fall within the bounds of Laplace–Lagrange secular theory. The divisors (3, 5, 21, 34) are all Fibonacci numbers, identified by exhaustive search over 7,558,272 possible Fibonacci d-assignments. Of these, 755 achieve an inclination balance above 99.994%; among those 755, only one is mirror-symmetric — the configuration used here.

4.4 Mirror Symmetry

Each inner planet shares its quantum number d with its outer counterpart across the asteroid belt: Mercury–Uranus (d = 21), Venus–Neptune (d = 34), Earth–Saturn (d = 3), Mars–Jupiter (d = 5). This mirror symmetry reflects the block-diagonal structure of the secular coupling matrix, with the asteroid belt acting as a dynamical barrier.

4.5 The Inclination Oscillation Mechanism

Each planet's inclination to the invariable plane oscillates as its ascending node precesses:

$$i(t) = \bar{i} + A\cos(\Omega(t) - \varphi_0) \tag{8}$$

where $\Omega(t) = \Omega_0 + (360°/P) \times t$ is the precessing ascending node and $\varphi_0 \approx 203.32°$ is a universal phase angle derived from the Laplace–Lagrange s_8 eigenmode. Saturn uses ~23.32° (offset by 180°) due to its retrograde nodal precession. The inclination oscillation is thus coupled to the ascending node precession — as the node completes one full circuit, the inclination completes one full oscillation cycle. This coupling is consistent with secular perturbation theory but emerges here from a single universal phase angle rather than per-planet fitting.

4.6 Law 3: The Inclination Balance

The angular-momentum-weighted inclination oscillations of seven planets balance against Saturn's alone, conserving the orientation of the invariable plane.

Each planet's orbital tilt oscillates with one of two phase angles (203° or 23°, derived from the s_8 eigenmode of secular perturbation theory):

- 203° **group**: Mercury, Venus, Earth, Mars, Jupiter, Uranus, Neptune
- 23° **group**: Saturn (alone, retrograde precession)

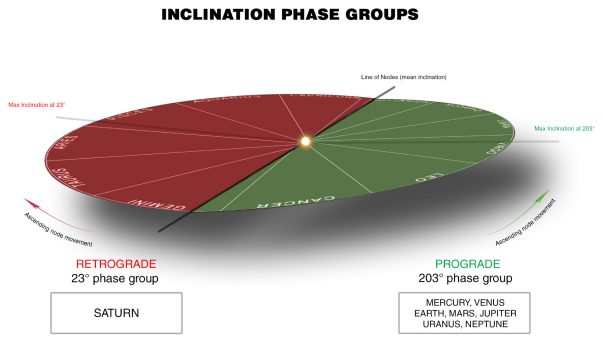

Figure 3: Inclination phase groups on the invariable plane. Seven planets (green) reach maximum inclination toward 203° with prograde ascending node precession; Saturn alone (red) reaches maximum inclination toward 23° with retrograde precession. At the line of nodes, each planet crosses through its mean inclination.

Saturn's orbital angular momentum — amplified by its large distance from the Sun — single-handedly balances the other seven planets combined. Using the structural weight $w_j = \sqrt{m_j \cdot a_j(1-e_j^2)}/d_j$, the balance is **99.9998%**. The tiny residual is well within the contribution of trans-Neptunian objects.

5. Laws 4–5: Eccentricity Structure

5.1 Law 4: The Eccentricity Constant

Within each mirror pair, the ratio of eccentricity to mean inclination satisfies two Fibonacci constraints that together determine all eight eccentricities from the inclinations alone.

For each planet, define $R = e/i_{\text{mean,rad}}$, measuring how it divides its orbital deviation between eccentricity (shape) and inclination (tilt). Within each mirror pair, R satisfies an R^2

sum constraint and a product or ratio constraint, providing two equations for two unknowns:

Table 4: Law 4: Fibonacci R^2 pair constraints (mean inclinations)

Mirror pair	$R_A^2 + R_B^2$	Second constraint	Type
Mars / Jupiter	$377/5 = 75.4$	$R_{\mathrm{Ma}} \times R_{\mathrm{Ju}} = 34/2 = 17$	Product
Earth / Saturn	$34/3 \approx 11.33$	$R_{\mathrm{E}} \times R_{\mathrm{Sa}} = 2$	Product
Venus / Neptune	$1/2 = 0.5$	$R_{\mathrm{V}}/R_{\mathrm{Ne}} = 2/8 = 0.25$	Ratio
Mercury / Uranus	$21/2 = 10.5$	$R_{\mathrm{Me}}/R_{\mathrm{Ur}} = 2/3$	Ratio

Belt-adjacent pairs use product constraints; outer pairs use ratio constraints — reflecting the different coupling regimes across the asteroid belt. Solving each pair predicts all eight eccentricities via $e = R \times i_{\mathrm{mean,rad}}$, with zero free parameters:

Table 5: Law 4: Eccentricity predictions from R^2 pair constraints

Planet	Predicted e	Reference e	vs. J2000
Mercury	0.2111	0.2056	+2.6%
Venus	0.00661	0.00678	−2.5%
Earth	0.01561	0.01532*	+1.9%
Mars	0.09320	0.09339	−0.2%
Jupiter	0.04853	0.04839	+0.3%
Saturn	0.05389	0.05386	+0.05%
Uranus	0.04709	0.04726	−0.4%
Neptune	0.00865	0.00859	+0.7%

* Base eccentricity (oscillation midpoint) from the 3D simulation. All other reference values are J2000 observed eccentricities; the model predicts base eccentricities, which may differ from J2000 snapshots (see text).

Total |error| across all eight planets: **8.57%** (average 1.07% per planet). These deviations may not be true errors: just as Earth's eccentricity oscillates around a base value of 0.015321 (distinct from its J2000 value of 0.01671), all planets have base eccentricities that differ from their J2000 snapshot. For most planets (Mars, Jupiter, Saturn, Uranus), the base eccentricity is within 0.2% of J2000; but for Mercury (+1.4%) and Neptune (+1.3%), the difference is significant — suggesting that part of the "error" reflects the J2000-to-base offset rather than a prediction failure. Earth's eccentricity, previously a free parameter (0.015321 from the 3D simulation midpoint), is now a predicted value at 1.9% accuracy. The inner planets also satisfy a Fibonacci ratio ladder: $\xi_V : \xi_E : \xi_{\mathrm{Ma}} : \xi_{\mathrm{Me}} = 1 : 5/2 : 5 : 8$, where $\xi = e \times \sqrt{m}$. Law 5 serves as an independent cross-check: the predicted eccentricities yield 99.93% balance. Monte Carlo tests confirm the constraints are genuinely independent of Law 5: among 150,000 random eccentricity sets satisfying the eccentricity balance, **zero** simultaneously reproduce the Fibonacci R^2 pair sums ($p < 10^{-5}$).

5.2 Dynamical Coupling: Earth–Saturn Communicating Vessels

The product constraint $R_{\mathrm{E}} \times R_{\mathrm{Sa}} = 2$ implies that Earth's and Saturn's eccentricities cannot evolve independently — they behave like communicating vessels. As Earth's eccentricity decreases toward its ∼0.0139 minimum (∼11,680 AD), R_{E} decreases, forcing R_{Sa} to increase and Saturn's eccentricity to rise. An observational clue supports this: Earth's eccentricity is currently decreasing while Saturn's is increasing — exactly as the product constraint predicts. The coupling is bidirectional: Saturn's own retrograde perihelion precession (period $H/8 = 41{,}736$ years) drives its own eccentricity changes, which feed back into Earth's eccentricity through the pair constraint. This unmodelled feedback may account for residual discrepancies between the model's eccentricity curve (which reflects only Earth's 20,868-year cycle) and formula-based predictions.

Quantifying the coupling. If $R_{\mathrm{E}} \times R_{\mathrm{Sa}} = 2$ holds as a dynamical invariant, then $e_{\mathrm{E}} \times e_{\mathrm{Sa}} = 2 \times i_{\mathrm{E,rad}} \times i_{\mathrm{Sa,rad}} \approx 0.00084$ at all times. Using the model's eccentricity range for Earth (0.0139–0.0167), the constraint predicts Saturn's eccentricity oscillates between ∼0.050 and ∼0.061. Conversely, Saturn's own $H/8$ cycle feeds back into Earth with an amplitude of $\sim \pm 0.0015$ — comparable to Earth's own eccentricity amplitude (0.0014). The combined effect would distort Earth's eccentricity curve from a pure sinusoid, potentially shifting the minimum depth and timing by several thousand years. Through the regression formula $Y_{\mathrm{sid}} = f(e)$, this translates to a Length of Day modulation of $\sim \pm 0.1$ ms from Saturn alone. Conventional secular theory gives Saturn's dominant eccentricity eigenfrequency (g_6) a period of ∼46,000 years — intriguingly close to $H/8 = 41{,}736$ years. Whether these represent the same physical period is testable against long-term numerical integrations.

A further consequence: because eccentricity determines the sidereal year length in days (Section 8.5), Saturn's influence on Earth's eccentricity indirectly affects both the length of Earth's year in days and the Length of Day — giving Saturn a measurable impact on the days and years experienced on Earth. The sidereal year *in seconds* is unaffected: it depends on Earth's semi-major axis (via Kepler's third law), not on eccentricity, and secular perturbations preserve semi-major axes to first order. Note also that the connection between Earth and Saturn is purely orbital: Saturn's *axial* precession (∼1.8 Myr, driven by a spin-orbit resonance with Neptune) is unrelated to the Fibonacci timescale hierarchy. Whether $R_{\mathrm{E}} \times R_{\mathrm{Sa}} = 2$ holds as a dynamical invariant is a testable prediction — as is the question of whether the same communicating-vessel behaviour holds for the other three mirror pairs (Mars/Jupiter, Venus/Neptune, Mercury/Uranus).

5.3 Law 5: The Eccentricity Balance

An independent balance condition on eccentricities holds using the same Fibonacci divisors and phase groups, with Saturn alone balancing the other seven planets.

Each planet receives an eccentricity weight $v_j = \sqrt{m_j} \times a_j^{3/2} \times e_j / \sqrt{d_j}$. The weights for the seven 203° planets sum to match Saturn's weight alone:

Balance: 99.88%

This is genuinely independent of Law 3: eccentricity weights differ from inclination weights by over 100-fold for some planets, yet both conditions are satisfied by the same Fibonacci divisors and phase assignment. Three tests confirm it depends on the actual eccentricity values: without eccen-

tricities the balance drops to 74%; random eccentricities give only 50–85%; and the balance peaks at linear eccentricity (99.88%), dropping to 91% for eccentricity squared.

Because Saturn is the only planet on one side, the balance equation directly predicts its eccentricity: 0.05373, compared with the observed value of 0.05386 (−0.24%).

Law convergence. Law 4 independently predicts Saturn's eccentricity from the R^2 pair constraint ($R^2_E + R^2_{Sa} = 34/3$): $e_{Saturn} = 0.05389$ (+0.05%). The two predictions bracket the J2000 value and differ by only 0.30%. Saturn's eccentricity oscillates secularly between ∼0.01 and ∼0.09 — a factor-of-9 dynamic range — yet two structurally different Fibonacci constraints, one using only the Earth–Saturn pair and the other using all eight planets, converge on the same value. The 8 pair constraints (Law 4) plus Law 5 provide 9 equations for 8 unknowns; the eccentricity balance is not imposed but emerges from the Fibonacci pair structure.

5.4 The Master Ratio $R \approx 311$

The ratio between the inclination and eccentricity scales — $R = \psi_1/\xi_{Venus} \approx 310.83$ — is close to the prime number 311. This number has special Fibonacci properties: 311 is a Fibonacci primitive root prime, meaning the golden ratio generates the entire multiplicative group modulo 311 (order 310 = maximum possible). Among all such primes, 311 is the closest to $R = 310.83$. R cannot be built from the quantum numbers $\{1, 3, 5, 8, 11, 13\}$ — it represents a genuinely external parameter connecting the eccentricity and inclination structures.

6. Law 6: Saturn-Jupiter-Earth Resonance

Saturn's retrograde precession creates a closed beat-frequency loop with Jupiter and Earth — the physical mechanism linking the Fibonacci timescale to orbital structure.

Saturn is the only planet with retrograde nodal precession, making it the natural pivot for both balance laws (Laws 3 and 5). Three beat-frequency relationships form a closed triangle:

Table 6: Law 6: Saturn-Jupiter-Earth beat-frequency resonance

Beat relationship	Fibonacci	Physical meaning
$\frac{1}{H/3} + \frac{1}{H/5} = \frac{1}{H/8}$	3 + 5 = 8	Earth incl. + Jupiter → obliquity (Saturn)
$\frac{1}{H/8} - \frac{1}{H/5} = \frac{1}{H/3}$	8 − 5 = 3	Saturn − Jupiter → Earth inclination
$\frac{1}{H/8} - \frac{1}{H/3} = \frac{1}{H/5}$	8 − 3 = 5	Saturn − Earth → Jupiter

All three rows are cyclic permutations of a single Fibonacci identity: 3 + 5 = 8. Each planet's period equals the beat frequency of the other two — Saturn ($H/8$) is the sum of Earth and Jupiter, Jupiter ($H/5$) is Saturn minus Earth, and Earth ($H/3$) is Saturn minus Jupiter. This also links to Law 1's higher-level identity 5 + 8 = 13: combining Jupiter ($H/5$) and Saturn ($H/8$) produces Earth's axial precession ($H/13$), extending the triangle into the full cycle hierarchy. Law 6 reveals the physical mechanism behind Law 1.

7. Statistical Significance and Exoplanet Evidence

7.1 Twelve Tests, Three Null Distributions

To address concerns first raised by Backus (1969) about Fibonacci structure in planetary systems, a comprehensive significance analysis was performed using twelve test statistics covering all six laws. Each was evaluated against three independent null distributions:

- **Permutation** (exhaustive 8! = 40,320 trials): same values, randomly reassigned to planets. Tests 11–12 are identity-dependent ($p = 1$ by construction).
- **Log-uniform Monte Carlo** (100,000 trials): random eccentricities and amplitudes from physical ranges, random d-values from Fibonacci sets.
- **Uniform Monte Carlo** (100,000 trials): same ranges, flat distribution.

Tests 5–7 use the model's fixed Fibonacci d-assignments and phase groups, ensuring **zero look-elsewhere effect**.

Table 7: Statistical significance of Fibonacci structure (12 tests)

Test	Observed	Perm.	Log-u.	Unif.
1. Pairwise count	**21/56**	**0.018**	**0.009**	**0.014**
2. Ecc. ladder	3	0.35	0.37	0.40
3. ψ (3-pl.)	16.97%	0.82	0.86	0.94
4. Cross-par.	5.43%	0.58	0.49	0.48
5. Incl. bal.	**99.9998%**	**5.7e-4**	**$< 10^{-5}$**	**$< 10^{-5}$**
6. Ecc. bal.	**99.88%**	**6.7e-4**	**3e-4**	**5e-4**
7. Saturn pred.	**0.24%**	**6.7e-4**	**3e-4**	**5e-4**
8. ψ full	**234.7%**	**0.047**	**0.017**	**0.027**
9. Prec. hier.	10 pr	0.83	0.91	0.79
10. R^2 part.‡	**4/4**	0.32	**9e-4**	**0.027**
11. E-J-S‡	**exact**	1	**0.033**	**0.032**
12. Mirror‡	**4/4**	1	**2e-4**	**2e-4**
Fisher's		**1.4×10^{-5}**	**7.1×10^{-14}**	**5.3×10^{-12}**

‡ Identity-dependent tests; permutation null cannot distinguish them.

Eight tests reach $p < 0.05$ across all applicable null distributions. Fisher's method gives a combined $p \leq 7.1 \times 10^{-14}$ (Monte Carlo) and $p = 1.4 \times 10^{-5}$ (conservative permutation). Tests 2–4 and 9 are individually non-significant, as expected from limited statistical power or circularity with model-derived amplitudes.

7.2 Exoplanet Evidence: TRAPPIST-1

The TRAPPIST-1 system provides independent evidence (Agol et al., 2021; Grimm et al., 2018):

- **Period ratios**: 5 of 6 consecutive period ratios match Fibonacci fractions (83%), the same percentage as the solar system
- **Fibonacci triad**: Mass-weighted eccentricities satisfy $3\xi_b + 5\xi_g = 8\xi_e$, using the same Fibonacci triple (3, 5, 8), holding to 0.34%
- **The number 311**: A super-period organizing the entire system equals $311 \times P_b$, with maximum deviation 0.12%

The same prime 311 appears independently as the solar system's master ratio $R = \psi_1/\xi_V \approx 310.83$. Monte Carlo simulations show $P \approx 2 \times 10^{-6}$ for this coincidence. Kepler-90 also shows 5 of 7 period ratios matching Fibonacci fractions (71%), though only two planets have measured masses.

Part II: Consequences for Earth

8. Observable Consequences for Earth

The six Fibonacci Laws produce specific, testable consequences for Earth's orbital dynamics. Each of Earth's known precession phenomena emerges from the model's two counter-rotating reference points.

8.1 Obliquity

The model's key structural insight is that observed obliquity is the sum of two oscillating components with equal amplitude:

$$\varepsilon(t) = \bar{\varepsilon} + A\cos\left(\frac{2\pi t}{T_{\text{axial}}}\right) + A\cos\left(\frac{2\pi t}{T_{\text{incl}}}\right) \tag{9}$$

where $\bar{\varepsilon} = 23.41398°$ (mean obliquity), $A = 0.633849°$ (amplitude), $T_{\text{axial}} = 25{,}683.69$ years, and $T_{\text{incl}} = 111{,}296$ years. The interaction produces a beat frequency with mean period ~41,736 years ($H/8$), matching the observed ~41,000-year obliquity cycle. Agreement with standard theory is excellent for ±10,000 years; beyond this range, the model predicts obliquity reversal after ~11,800 AD while Laskar's polynomial predicts continued decrease (Fig. 4).

Table 8: Obliquity: model vs. standard theory

Year	Model	Laskar 1993	Chapront et al. 2002	Diff.
2000 AD	23.4392°	23.4392°	23.4392°	0.000°
10,000 BC	24.51°	24.17°	24.3°	~0.2°
10,000 AD	22.61°	22.65°	22.64°	~0.04°

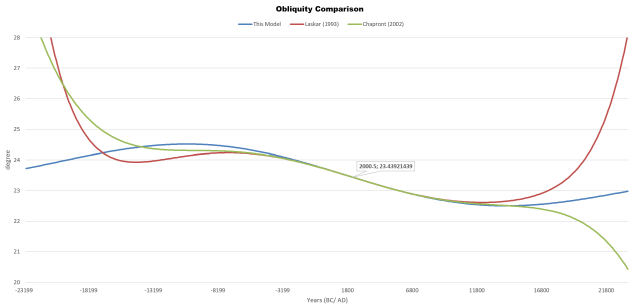

Figure 4: Obliquity predictions compared: this model (blue) versus Laskar (1993) (red) and Chapront et al. (2002) (green). Polynomial extrapolations diverge to unphysical values (20°–28°), while the model predicts bounded oscillation within 22.2°–24.7°.

The model's inclination precession cycle (~111,296 years) is independently validated by comparison with Vieira et al. (2012), who computed Earth's inclination relative to the invariable plane over 600 kyr (Fig. 5). Both show oscillation between ~0.5° and ~2.5°.

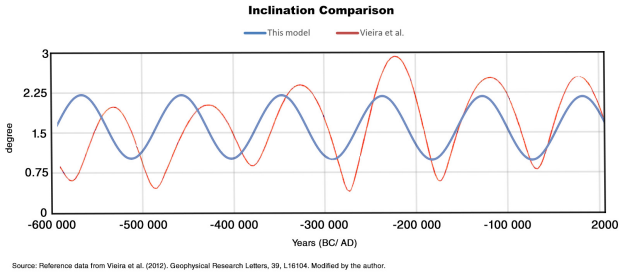

Figure 5: Orbital inclination compared: this model (blue) versus Vieira et al. (2012) (red). Both show oscillation between ~0.5° and ~2.5° with the ~111,296-year period.

8.2 Eccentricity: The 20,868-Year Cycle

In contrast to Milankovitch's ~95,000/125,000/400,000-year eccentricity cycles, the model proposes a single 20,868-year cycle. As the two reference points orbit in opposite directions, the effective distance between them oscillates with their meeting frequency. Current eccentricity: 0.01671 (J2000). Base eccentricity: 0.015321. Amplitude: ±0.0014226. Range: 0.0139–0.01674. Next minimum: ~11,680 AD (Fig. 6).

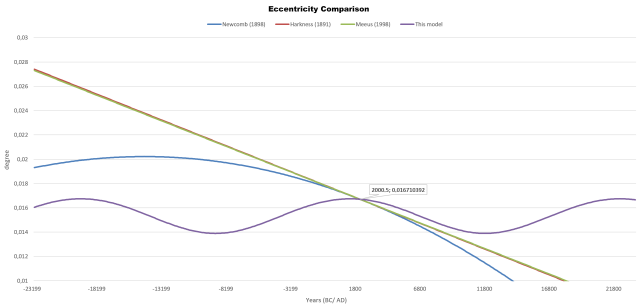

Figure 6: Eccentricity predictions: this model (purple) versus polynomials from Newcomb (1898) (blue), Harkness (1891) (red), and Meeus (1998) (green). Standard theory predicts decrease toward ~0.01; the model predicts bounded oscillation with minimum at ~11,680 AD.

Note: this eccentricity curve reflects only Earth's own 20,868-year perihelion cycle. Law 4 (Section 5) shows that Earth and Saturn form a mirror pair with the product constraint $R_{\text{E}} \times R_{\text{Sa}} = 2$, coupling their eccentricities like communicating vessels. Saturn's own retrograde perihelion precession (41,736 years) drives additional eccentricity changes that feed back into Earth's through this constraint — an effect not yet incorporated into the curve above.

8.3 Longitude of Perihelion

The longitude of perihelion advances through all 360° once per 20,868-year cycle, currently at 102.95° (J2000). Comparison with Meeus (1998) shows close agreement for ±3,000 years (±0.03° at 1000 AD, ±0.09° at 2500 AD); beyond this range the predictions diverge (Fig. 7).

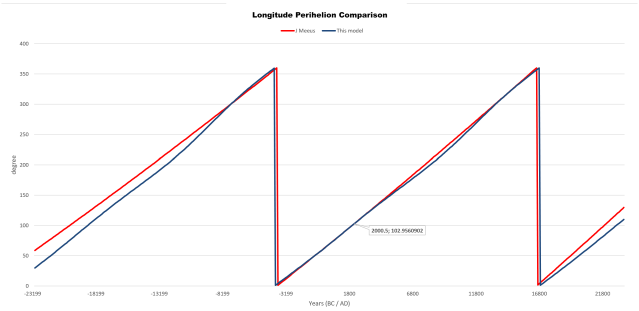

Figure 7: Longitude of perihelion: this model (blue) versus Meeus (1998) polynomial (red). Close agreement for ±3,000 years around J2000.

8.4 Length of Day and Timekeeping

Standard theory attributes Earth's rotational slowing to lunar tidal friction (~2.3 ms/century), predicting monotonic increase in LOD. The model proposes an additional cycle superimposed on tidal slowing, following the 20,868-year perihelion precession cycle (Table 9). Currently, the model predicts LOD is in a decreasing phase (Earth speeding up). Earth unexpectedly began rotating faster in 2020, with the shortest day ever recorded on June 29, 2022 (1.59 ms under 24 hours) — qualitatively consistent with the model's prediction.

Table 9: Length of Day: current vs. mean values

Parameter	Current value	Mean value
Solar day	~86,400.0003 s	86,399.9886 s
Sidereal day	~86,164.0905 s	86,164.0793 s

Mitchell & Kirscher (2023) demonstrated that Earth's day length stalled at approximately 19 hours for roughly 1 billion years during the mid-Proterozoic, likely due to atmospheric thermal tides balancing lunar tidal deceleration. This proves that LOD dynamics are more complex than simple tidal deceleration and that additional mechanisms can influence Earth's rotation over geological timescales.

8.5 Obliquity & Eccentricity Define Lengths of Days & Years

Regression analysis across 27,000 years of simulation data yields three closed-form formulas. **Tropical year from obliquity** ($R^2 = 0.9995$):

$$Y_{\text{trop}} = \bar{Y}_{\text{solar}} - \frac{k_1}{\bar{D}} \times (\varepsilon - \bar{\varepsilon}) \tag{10}$$

where $k_1 = 2.3$ s/degree. **Sidereal year (in days) from eccentricity** ($R^2 = 0.9996$):

$$Y_{\text{sid}} = \bar{Y}_{\text{sid}} - \frac{k_2}{\bar{D}} \times (e - \bar{e}) \tag{11}$$

where $k_2 = 3208$ s/unit eccentricity and $\bar{e} = 0.01539 = \sqrt{e_0^2 + A_e^2}$. **Length of Day** follows from the sidereal year being fixed at 31,558,149.724 seconds:

$$D = \frac{31{,}558{,}149.724}{Y_{\text{sid}}(\text{days})} \tag{12}$$

The two formulas reveal a clean separation of roles. The tropical year is almost entirely determined by obliquity ($R^2 = 0.9995$), while eccentricity has negligible effect ($R^2 = 0.0005$). Conversely, the sidereal year in days is determined by eccentricity ($R^2 = 0.9996$): the sidereal year *in seconds* is fixed at 31,558,149.724 s (Earth's orbital period relative to fixed stars, preserved by Kepler's third law), but changing eccentricity changes the day length, which changes how many days fit into that fixed number of seconds. The day length varies ±4–5 ms over the 20,868-year perihelion cycle. Additionally, tropical years measured at different cardinal points differ by up to ~45 seconds due to eccentricity effects, with the pattern rotating through the seasons over the perihelion cycle.

8.6 The Coin Rotation Paradox

The model reveals structural relationships between different measures of days and years (Table 10).

Table 10: Types of days and years

Type	Reference	Duration
Solar day	Sun's apparent position	~86,400 s
Sidereal day	Precessing equinox	~86,164.09 s
Stellar day	Fixed stars (ICRF)	~86,164.10 s
Solar year	Equinox to equinox	~365.2422 d
Sidereal year	Fixed stars	31,558,149.724 s
Anomalistic year	Perihelion to perihelion	~365.2597 d

The difference between stellar and sidereal day, and between sidereal and solar year, are direct consequences of axial precession. The precession rate varies over the Holistic cycle: the cycle-averaged mean period is ~25,684 years, while the current instantaneous period is ~25,772 years. Using mean values, each difference accumulates to exactly one fewer unit per cycle:
Day level:

$$9.16 \text{ ms/sid. day} \times 366.25 \text{ sid. days/yr} \times 25{,}684 \text{ yr} \approx 86{,}164 \text{ s} = 1 \text{ sidereal day} \tag{13}$$

Year level:

$$1{,}228.72 \text{ s/yr (mean solar–sidereal year diff.)} \times 25{,}684 \text{ yr} \approx 31{,}558{,}150 \text{ s} = 1 \text{ sidereal year} \tag{14}$$

The coin rotation paradox (a coin rolling around an identical coin makes 2 rotations, not 1) manifests at these two scales:

- **Daily**: 366.25 sidereal days = 365.25 solar days per year (one extra stellar rotation from orbital motion)
- **Yearly**: 25,683 sidereal years = 25,684 solar years per axial precession cycle (one fewer sidereal year from the precession orbit)

This self-consistency check links the model's precession period to its day/year length formulas.

9. The 100,000-Year Problem: Inclination as Climate Driver

9.1 Inclination Precession as Climate Driver

The model proposes that the dominant ~100,000-year periodicity in ice core records (Hays et al., 1976) reflects the inclination precession cycle (~111,296 years) rather than eccentricity. Three inclination precession cycles span one Holistic-Year ($3 \times 111{,}296 = 333{,}888$), producing the three major glacial sub-cycles visible in Antarctic ice core data (Fig. 8). The ~10% discrepancy between the observed ~100,000-year signal and the predicted ~111,296-year cycle may fall within ice core dating uncertainties.

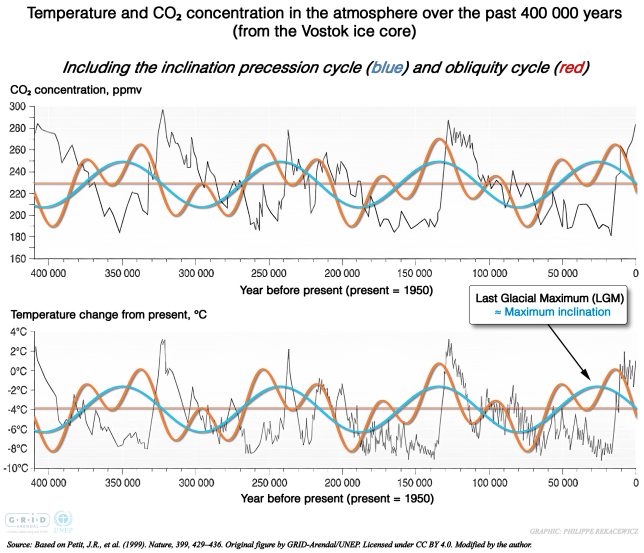

Figure 8: Vostok ice core temperature and CO_2 data with the model's inclination precession cycle (~111,296 years, blue) and obliquity cycle (~41,000 years, red) overlaid. Three inclination cycles span one Holistic-Year (333,888 years), corresponding to the three major glacial–interglacial transitions. Background data from Petit et al. (1999), CC BY 4.0; model curves by the author.

9.2 Peer-Reviewed Support: Muller & MacDonald (1997)

Muller & MacDonald (1997b), published in PNAS, demonstrated three key findings: (1) the eccentricity spectrum shows split peaks at ~95 ka and ~125 ka while climate shows a single narrow peak near ~100 ka; (2) eccentricity's dominant ~400 ka component is largely absent from climate records; (3) inclination provides a better spectral match including phase relationships. Their proposed mechanism (interplanetary dust) was rejected, but their spectral evidence has never been refuted.

9.3 Ice Core Chronology and the Mid-Pleistocene Transition

Many ice core chronologies employ orbital tuning — adjusting timescales to match Milankovitch insolation — creating circularity. Modern chronologies (AICC2012; Veres et al. 2013) minimize this through annual layer counting, volcanic markers, and U-series dating (Kawamura et al., 2007), but for ice older than ~400 ka, orbital tuning remains significant.

The model's balanced state appears to have existed for approximately 1 million years, coinciding with the Mid-Pleistocene Transition (~1.2–0.7 Ma). Before this, climate records show a dominant ~41,000-year cycle; after, the ~100,000-year pattern emerged. This transition may mark the onset of the current Fibonacci-ratio synchronization. The model makes no claim about when this regime will end — dynamical transitions are inherently unpredictable (Laskar, 1993).

10. Mercury's Perihelion: A Reference Frame Consequence

10.1 Standard Framework and Alternative Interpretation

Mercury's perihelion precesses at 575.31 ± 0.0015″/cy (ICRF) (Park et al., 2017). Newtonian perturbations account for ~532″/cy; the remaining ~43″ has been attributed to General Relativity since 1915. The model proposes this discrepancy arises from Earth's reference frame motion rather than space-time curvature: Earth's precession motions create a moving observation platform, and the model predicts this effect was ~43″ around 1900 but is decreasing (Table 11).

Table 11: Mercury precession: model predictions over time

Year	Geocentric (″/cy)	ICRF (″/cy)	"Anomaly"
1800	~5,609	~580	~47″
1900	~5,605	~577	~43″
2000	~5,601	~573	~39″
2100	~5,597	~568	~34″

In the geocentric frame, the full Clemence (1947) breakdown (as reviewed by Berche & Medina 2024) shows Venus contributing ~278″/cy (52%), Jupiter ~154″/cy (29%), Earth ~90″/cy (17%), Saturn ~7″/cy, and Mars + others ~3″/cy, giving a Newtonian subtotal of 5,557.18 ± 0.85″/cy against an observed 5,599.74 ± 0.41″/cy — leaving a residual of 42.56 ± 0.94″/cy. The uncertainty on this residual (~1″/cy) is rarely emphasized.

The model does not claim GR is incorrect — only that this particular observational test may have an alternative geometric interpretation. As noted by Krizek & Somer (2023), "the definitive proof of these famous theories is still to be delivered." The model implements Laplace–Lagrange secular theory, reproducing the standard Newtonian breakdown with ~96% accuracy. A notable failure occurs for Venus: secular theory predicts 1,075″/cy versus the observed 204″/cy. This is a known limitation of first-order secular theory for low-eccentricity orbits — Venus's nearly circular orbit ($e = 0.007$) makes its perihelion direction extremely sensitive to perturbations. This connects to the finding (Section 11) that low-eccentricity planets' precession fluctuations are dominated by Earth's rate variations rather than geometric modulation — both observations reflect the same physics: perihelion is poorly defined for nearly circular orbits.

10.2 Independent N-Body Convergence

Three independent approaches converge at epoch J2000:

Table 12: Mercury geocentric precession: three independent sources

Source	Method	Total (″/cy)
Smulsky (2011)	Galactica N-body	5,601.9
Berche & Medina (2024)	Analytical (Clemence, 1947)	5,599.7
This model	Geometric framework	5,601.34

10.3 The Beat-Frequency Structure

The model predicts Mercury's Earth-frame precession rate oscillates with a dominant period of ~7,420 years (1/45 of the Holistic-Year). The fluctuation ranges from −157″ to +174″/cy around the ~534″ baseline. When measured in the ecliptic frame, Mercury's rate is constant at ~533.7″/cy — the fluctuation appears only in the Earth-frame measurement and averages to zero over the full Holistic-Year.

10.4 The BepiColombo Test

MESSENGER measured 575.31 ± 0.0015″/cy at epoch ~2013. BepiColombo (orbit insertion November 2026, science operations from April 2027) will provide the second high-precision epoch (Table 13):

Table 13: BepiColombo prediction: model vs. GR

Theory	Value	Diff. from MESSENGER
Model	~574.69″/cy	−0.62″/cy (~400× unc.)
GR	~575.31″/cy	constant (no change)

The model predicts the rate decreases by ~0.045″/cy per year. Over ~14 years (MESSENGER → BepiColombo), the decrease of ~0.6″/cy is well within BepiColombo's capability. The Sun's gravitational quadrupole moment (J_2), which varies with solar activity (Mecheri & Abdelatif, 2022), creates a systematic uncertainty that BepiColombo will help resolve.

10.5 The Measurement Chain: An Open Question

The 575″/cy value is reported as Mercury's precession "relative to ICRF." However, the measurement chain depends critically on Earth's position in ICRF, which is calculated from Earth orientation models that account for precession, nutation, and polar motion. If Earth's long-period precession motions (~25,684 and ~111,296 year cycles) have any systematic modeling errors, these would propagate into Mercury's calculated position. The model proposes that the *interference pattern* between two known long-period cycles produces time-dependent residuals not fully captured by standard IAU precession corrections.

Part III: Predictions and Validation

11. Unified Predictive Formulas

A unified 273-term formula system predicts the precession fluctuation of all seven planets (excluding Earth, the observer) using only time as input — no observation of each planet's perihelion is required. The system uses Earth's formulas (perihelion longitude, obliquity, eccentricity, Earth Rate Deviation) to predict how each planet's *apparent* precession changes due to Earth's reference frame motion.

Table 14: Unified predictive formula performance

Planet	R^2	RMSE (″/cy)	Base (″/cy)	Period (yr)
Mercury	0.9990	2.44	533.7	242,828 (H×8/11)
Venus	0.9983	21.64	194.1	667,776 (H×2)
Mars	0.9999	0.75	1,682.0	77,051 (H×3/13)
Jupiter	0.9999	0.52	1,940.8	66,778 (H/5)
Saturn	1.0000	0.29	−3,105.2	41,736 (H/8, retr.)
Uranus	0.9999	0.28	1,164.5	111,296 (H/3)
Neptune	0.9999	0.20	194.1	667,776 (H×2)

All planets are predicted with > 99.8% accuracy across the full 333,888-year Holistic cycle.

11.1 Eccentricity-Dependent Driver Mechanisms

The analysis reveals that different planets show fundamentally different fluctuation drivers:

- **Mercury** (e = 0.206): Well-defined perihelion. Dominated by geometric modulation — angular interference of Earth's and Mercury's perihelion precessions.
- **Venus** (e = 0.007): Poorly defined perihelion. Dominated by quadratic Earth Rate Deviation effects.
- **Mars through Neptune**: Dominated by linear rate-cycle interactions.

This eccentricity dependence is a natural consequence of the reference frame interpretation.

11.2 Saturn as the Obliquity Driver

Saturn is the only planet requiring time-varying obliquity and eccentricity parameters for accurate predictions. Its precession period (41,736 years = H/8) exactly equals Earth's obliquity cycle — a resonance, not a coincidence. Without time-varying coupling terms, Saturn's formula cannot achieve R^2 = 1.0, suggesting Saturn's precession directly modulates Earth's axial tilt oscillation.

12. Calibration, Validation, and Transparency

12.1 Free Parameters

The model has 6 adjustable parameters — 5 for the Earth simulation and 1 discrete configuration choice for the planetary Fibonacci structure:

Table 15: Free parameters

Parameter	Value	How determined
Holistic-Year	333,888 yr	Fitted to 1246 AD alignment + J2000 longitude
Fibonacci divisors	3, 8, 13	Structural assumption
Mean obliquity	23.41398°	Fitted to observed obliquity range
Amplitude	0.633849°	Fitted to observed obliquity range
Anchor year	−301,340	Derived from Holistic-Year and 1246 AD
Planet configuration	Config #32	Exhaustive search; unique mirror-symmetric solution

The planet configuration assigns three quantities to each planet: an oscillation period (from Law 1's Fibonacci hierarchy), a quantum number d (determining amplitude via Law 2), and a phase angle (prograde or retrograde). The periods and phases are observationally constrained; only the d-assignment is a free choice, making this a single discrete parameter.

Table 16: Genuine predictions (not used in calibration)

Prediction	Model	Reference value	Agreement
Obliquity at 9,188 BC	24.30°	24.12° (Laskar)	±0.18°
Obliquity at 11,680 AD	22.33°	22.37° (Laskar)	±0.04°
Perihelion long. 1000 AD	85.77°	85.8° (Meeus)	±0.03°
Eccentricity (J2000)	0.01671	0.01671022 (NASA)	±0.00001
Incl. to inv. plane	1.5787°	1.5787° (S&S 2012)	±0.0001°

12.2 Ascending Node Calibration

The inclination oscillation formula requires accurate ascending node positions on the invariable plane. Souami & Souchay (2012) published these for all planets, but a systematic issue arises: their values are calibrated to epoch-specific inclinations, while the model uses mean (time-averaged) inclinations. When Earth's mean inclination (1.482°) is used instead of the J2000 value (1.579°), the original S&S ascending nodes produce ecliptic inclinations that deviate from observed JPL values. Using spherical trigonometry:

$$\cos(i_{\text{ecl}}) = \cos(i_p)\cos(i_e) + \sin(i_p)\sin(i_e)\cos(\Delta\Omega) \quad (15)$$

where i_p and i_e are the planet's and Earth's inclinations to the invariable plane, and $\Delta\Omega$ is the ascending node difference. Since i_{ecl} is known from JPL observations, the ascending node becomes the only unknown — geometrically determined, not a free parameter. Two independent methods — numerical optimization and analytical solution — produce identical results (Table 17).

Table 17: Ascending node calibration results

Planet	S&S (°)	Verified (°)	Δ (°)	JPL (°)	Error
Mercury	32.22	32.83	+0.61	7.005	< 0.0001°
Venus	52.31	54.70	+2.39	3.395	< 0.0001°
Mars	352.95	354.87	+1.92	1.850	< 0.0001°
Jupiter	306.92	312.89	+5.97	1.303	< 0.0001°
Saturn	122.27	118.81	−3.46	2.485	< 0.0001°
Uranus	308.44	307.80	−0.64	0.773	< 0.0001°
Neptune	189.28	192.04	+2.76	1.770	< 0.0001°

This calibration is not circular reasoning: JPL ecliptic inclinations are observed (spacecraft tracking), S&S invariable plane inclinations are independently derived (angular momentum calculations), and the ascending node is determined by the geometry linking these two independent datasets.

12.3 Historical Observation Validation

The 3D simulation has been validated against over 700 historical astronomical observations spanning ~2000 BC to ~4000 AD: Mercury and Venus transits (~190 events), Mars oppositions (~140), Jupiter–Saturn great conjunctions (~150), and mutual planetary occultations (~100). Accuracy: < 1′ for the current epoch (±100 yr), < 5′ for historical (±1,000 yr), < 15′ for ancient (> 2,000 yr).

12.4 Comparison with JPL DE440/441

The JPL Development Ephemeris (DE440/441; Park et al. 2021) is the gold standard for solar system dynamics.

Table 18: Obliquity predictions: model vs. DE441/Laskar

Year	Model	DE441/Laskar	Diff.
1000 BC	23.98°	24.02°	−0.04°
J2000	23.439°	23.439°	0 (calib.)
3000 AD	23.53°	23.52°	+0.01°
5000 AD	23.54°	23.53°	+0.01°
10,000 AD	22.89°	22.84°	+0.05°
20,000 AD	22.69°	22.62°	+0.07°

Agreement is excellent for ±5,000 years, with divergence reaching ~0.1° by 20,000 AD.

Table 19: Eccentricity predictions: model vs. Laskar et al. 2004 — the primary differentiating prediction

Year	Model	Laskar et al. 2004	Diff.
J2000	0.01671	0.01671	0 (calib.)
5,000 AD	0.0163	0.0161	+0.0002
11,680 AD	**0.0139** (min)	0.0152	−0.0013
27,000 AD	0.0163	~0.005 (min)	+0.011

The model predicts eccentricity minimum of ~0.0139 at 11,680 AD versus Laskar's continued decrease toward ~0.005 at 27,000 AD — a divergence larger than half the current eccentricity. For timescales beyond ~2,000 years, neither the model nor DE440/441 can be directly verified — both are extrapolations.

12.5 Error Analysis

Uncertainties propagate from the 6 free parameters. The dominant source is the obliquity amplitude (±0.01°), which grows linearly with time. Table 20 shows propagated uncertainties at two future epochs.

Table 20: Propagated uncertainties at future epochs

Epoch	Obliquity	Eccentricity
Yr 3000 (J2000 + 1 ka)	23.53° ± 0.02°	0.0166 ± 0.0001
Yr 12000 (J2000 + 10 ka)	22.41° ± 0.2°	0.0142 ± 0.001

13. Testable Predictions

The model generates 17 specific predictions:

13.1 Near-Term (Decades)

1. **Axial precession period**: Will stabilize near current value before decreasing — not the monotonic decrease predicted by Capitaine et al. (2003).
2. **Mercury perihelion anomaly**: Geocentric precession will decrease from ~5,601″/cy (2000) toward ~5,597″/cy (2100).
3. **RA at maximum declination**: The Sun's ICRF right ascension at summer solstice peaked at exactly 6h in 1246 AD and is now shifting.
4. **Jupiter and Saturn perihelion trends**: Current trends will continue without pattern change.
5. **Neptune ecliptic inclination**: The model predicts a decrease, while current JPL trend figures show an increase. This is the only planet where the model and JPL disagree on the direction of inclination change — a clean, decisive near-term test.

13.2 Medium-Term (Centuries)

6. **Obliquity divergence** after ~11,800 AD: model predicts reversal; standard theory predicts continued decrease.
7. **Longitude of perihelion divergence** after ~3,000 AD.
8. **Gregorian calendar drift**: June solstice on June 18 by ~11,680 AD.
9. **Analemma shape changes** with eccentricity and obliquity cycles.

13.3 Long-Term (Millennia)

10. **Eccentricity minimum at** ~11,680 **AD**: ~0.0139, then increasing. Key differentiator from Milankovitch theory.
11. **Inclination minimum at** ~32,548 **AD**: ~0.848° to invariable plane.
12. **Length of Day reversal**: LOD will decrease until ~11,680 AD.
13. **Solar year in days**: Will increase until ~13,800 AD.
14. **Sidereal year in seconds**: Fixed at 31,558,149.724 s.
15. **All precession movements related**: Follow a unified pattern repeating every 20,868 years.
16. **Invariable plane tilt**: Mean = 1.481592° with ±0.634° amplitude.
17. **Long-term temperature decline**: As inclination tilt decreases, longer glacial periods.

13.4 Falsification Criteria

The model would be falsified if:

- Eccentricity is unbounded: the core prediction is a bounded oscillation ($e \gtrsim 0.013$) on the perihelion timescale, not the continued decrease toward ~0 of Milankovitch theory. Earth–Saturn coupling (Section 5) may shift the exact minimum from the nominal ~0.0139 at ~11,680 AD, but the oscillation must remain bounded.
- The ~100,000-year climate cycle is proven eccentricity-driven
- Mercury's geocentric precession remains constant at ~5,604″/cy over decades

14. Discussion

14.1 What the Model Explains

The Holistic Universe Model unifies six phenomena — axial precession, inclination precession, perihelion precession, obliquity variation, eccentricity variation, and day/year length changes — within a single geometric framework. Beyond Earth, six Fibonacci Laws connect the orbital properties of all eight planets through a single timescale. The framework produces closed-form formulas for any epoch, eliminating the need for numerical integration within its domain of applicability.

14.2 Relationship to Existing Theory

The model does not contradict Newtonian gravity. It proposes that the long-term behavior of planetary parameters may be captured by a geometric description that reveals Fibonacci structure — consistent with KAM theory's prediction that maximally stable orbits have frequency ratios converging to the golden ratio.

14.3 Limitations

The model does not explain:

- **Why** the Fibonacci ratio 13:3 exists
- **Why** 333,888 specifically
- **What physical mechanism** produces equal obliquity amplitudes
- Short-term perturbations or chaotic orbital evolution

The model describes secular (long-term) trends only. It does not include short-period perturbations that average to zero over millennial timescales:

Table 21: Physical effects not included in the model

Perturbation	Period	Effect	Treatment
Lunar nodal cycle	18.6 yr	±9″ nutation	Averaged out
Chandler wobble	~433 d	Axis wobble (0.7″)	Not modeled
Annual wobble	1 yr	Seasonal mass redistrib.	Not modeled
Jupiter perturbations	~11.86 yr	Orbital variations	Averaged out
Saturn perturbations	~29.5 yr	Orbital variations	Averaged out
Solar activity cycle	~11 yr	Minor thermal effects	Not modeled

For the model's primary predictions (obliquity, eccentricity, longitude of perihelion over millennia), these perturbations contribute $< 0.01°$ to obliquity, < 0.0001 to eccentricity, and $< 0.1°$ to longitude — within the model's stated uncertainties. For precise positions on any given day, standard ephemerides (JPL DE440/441) should be used. The model's configuration applies from ~1 million years ago (Mid-Pleistocene Transition) to the present epoch.

14.4 The Overfitting Concern

With 6 free parameters (5 continuous, 1 discrete configuration), overfitting is addressed by:

1. Explicitly separating calibration from predictions (Section 12)
2. Agreement with values not used in construction (eccentricity, invariable plane inclination, ascending nodes to $< 0.0001°$)
3. 17 testable predictions, several falsifiable within decades
4. $R^2 > 0.998$ for all 7 planets using a single formula structure
5. Six Fibonacci Laws predicting orbital properties with zero free parameters, confirmed by exoplanet evidence

15. Conclusions

We have presented six Fibonacci Laws of planetary motion derived from a unified geometric model. The laws connect a single timescale — the 333,888-year Holistic-Year, produced by two counter-rotating reference points in a 13:3 ratio — to the orbital properties of all eight planets:

1. **Law 1**: The Holistic-Year divided by Fibonacci numbers generates all major precession periods
2. **Law 2**: A universal inclination constant, derived from Fibonacci numbers and H, predicts all eight planets' tilt amplitudes with zero free parameters (max error 0.16%)
3. **Law 3**: Angular-momentum-weighted inclination oscillations balance to 99.9998%
4. **Law 4**: Fibonacci pair constraints on the AMD partition ratio predict all eight eccentricities from inclinations alone (zero free parameters, max error 2.6%)
5. **Law 5**: An independent eccentricity balance predicts Saturn's eccentricity to 0.24%
6. **Law 6**: A Saturn-Jupiter-Earth resonance loop closes the structure through the Fibonacci identity $3 + 5 = 8$

Twelve statistical tests yield Fisher's combined $p \leq 7.1 \times 10^{-14}$, with independent confirmation from TRAPPIST-1 ($P \approx 2 \times 10^{-6}$ for the 311 coincidence). These laws produce specific consequences for Earth: a unified obliquity formula matching standard theory to $\pm 0.04^{\circ}$ over $\pm 10{,}000$ years, a 20,868-year eccentricity cycle, a resolution of the 100,000-year problem through inclination precession, and a decreasing Mercury perihelion anomaly testable by BepiColombo (~574.69″/cy versus MESSENGER's 575.31″/cy, science operations from April 2027).

A unified 273-term formula system predicts planetary precession with $R^2 > 0.998$ for all 7 planets. The model uses 6 free parameters and is fully transparent about calibration versus prediction. The model, interactive 3D simulation, and complete formula derivations are freely available at https://holisticuniverse.com.

Acknowledgments

The author thanks the developers of JPL Horizons, WebGeocalc, and the IAU standards for providing the observational data upon which this model is built. The interactive 3D simulation was built using Three.js and is available at https://3d.holisticuniverse.com. The source code is available at https://github.com/dvansonsbeek/3d.

Data Availability

All data, formulas, and calculation scripts underlying this work are publicly available:

- Documentation and formulas: https://holisticuniverse.com/reference/formulas
- Interactive 3D simulation: https://3d.holisticuniverse.com
- Data visualization: https://data.holisticuniverse.com
- Source code: https://github.com/dvansonsbeek/3d

Conflict of Interest

The author declares no conflicts of interest. This research received no external funding.

References

Agol, E., Dorn, C., Grimm, S. L., et al. (2021). Refining the Transit-timing and Photometric Analysis of TRAPPIST-1: Masses, Radii, Densities, Dynamics, and Ephemerides. *The Planetary Science Journal*, 2(1), 1.

Aschwanden, M. J. (2018). Self-organizing systems in planetary physics: Harmonic resonances of planet and moon orbits. *New Astronomy*, 58, 107–123.

Backus, G. (1969). Critique of "The Resonant Structure of the Solar System" by A. M. Molchanov. *Icarus*, 11, 88–92.

Barker, S., Lisiecki, L. E., Knorr, G., Nuber, S., & Tzedakis, P. C. (2025). Distinct roles for precession, obliquity, and eccentricity in Pleistocene 100-kyr glacial cycles. *Science*, 387(6737), eadp3491.

Berche, B., & Medina, E. (2024). The advance of Mercury's perihelion: a historical review. *arXiv:2402.04643*.

Berger, A. (1988). Milankovitch theory and climate. *Reviews of Geophysics*, 26(4), 624–657.

Capitaine, N., Wallace, P. T., & Chapront, J. (2003). Expressions for IAU 2000 precession quantities. *Astronomy & Astrophysics*, 412, 567–586.

Chapront, J., Chapront-Touzé, M., & Francou, G. (2002). Expressions for the Celestial Intermediate Pole and Celestial Ephemeris Origin consistent with the IAU 2000A precession-nutation model. *Astronomy & Astrophysics*, 387, 700–709.

Clemence, G. M. (1947). The relativity effect in planetary motions. *Reviews of Modern Physics*, 19(4), 361–364.

Greene, J. M. (1979). A method for determining a stochastic transition. *Journal of Mathematical Physics*, 20(6), 1183–1201.

Grimm, S. L., Demory, B.-O., Gillon, M., et al. (2018). The nature of the TRAPPIST-1 exoplanets. *Astronomy & Astrophysics*, 613, A68.

Harkness, W. (1891). The Solar Parallax and Its Related Constants (Washington: Government Printing Office).

Hays, J. D., Imbrie, J., & Shackleton, N. J. (1976). Variations in the Earth's orbit: Pacemaker of the ice ages. *Science*, 194(4270), 1121–1132.

Kawamura, K., Parrenin, F., Lisiecki, L., et al. (2007). Northern Hemisphere forcing of climatic cycles in Antarctica over the past 360,000 years. *Nature*, 448, 912–916.

Krizek, M., & Somer, L. (2023). *Mathematical Aspects of Paradoxes in Cosmology*. Springer.

Laskar, J. (1993). Orbital, precessional and insolation quantities for the Earth from −20 Myr to +10 Myr. *Astronomy & Astrophysics*, 270, 522–533.

Laskar, J. (1997). Large scale chaos and the spacing of the inner planets. *Astronomy & Astrophysics*, 317, L75–L78.

Laskar, J., Robutel, P., Joutel, F., et al. (2004). A long-term numerical solution for the insolation quantities of the Earth. *Astronomy & Astrophysics*, 428, 261–285.

Mecheri, R., & Abdelatif, T. (2022). Secular Variations of the Sun's Gravitational Quadrupole Moment and Their Impact on GR Tests. *Remote Sensing*, 14(19), 4798.

Meeus, J. (1998). *Astronomical Algorithms*, 2nd edn. (Richmond: Willmann-Bell).

Mitchell, R. N., & Kirscher, U. (2023). Mid-Proterozoic day length stalled by tidal resonance. *Nature Geoscience*, 16, 567–569.

Morbidelli, A., & Giorgilli, A. (1995). Superexponential stability of KAM tori. *Journal of Statistical Physics*, 78, 1607–1617.

Muller, R. A., & MacDonald, G. J. (1997a). Glacial cycles and astronomical forcing. *Science*, 277, 215–218.

Muller, R. A., & MacDonald, G. J. (1997b). Spectrum of 100-kyr glacial cycle: Orbital inclination, not eccentricity. *Proceedings of the National Academy of Sciences*, 94, 8329–8334.

Newcomb, S. (1898). Tables of the Motion of the Earth on its Axis and Around the Sun, Astronomical Papers, Vol. VI (Washington: US Naval Observatory).

Park, R. S., Folkner, W. M., Konopliv, A. S., et al. (2017). Precession of Mercury's perihelion from ranging to the MESSENGER spacecraft. *The Astronomical Journal*, 153(3), 121.

Park, R. S., et al. (2021). The JPL planetary and lunar ephemerides DE440 and DE441. *The Astronomical Journal*, 161(3), 105.

Petit, J. R., Jouzel, J., Raynaud, D., et al. (1999). Climate and atmospheric history of the past 420,000 years from the Vostok ice core, Antarctica. *Nature*, 399, 429–436.

Pletser, V. (2019). Fibonacci numbers and the golden ratio in biology, physics, astrophysics, chemistry and technology: a non-exhaustive review. *Astrophysics and Space Science*, 364, 158.

Smulsky, J. J. (2011). New components of the Mercury's perihelion precession. *Natural Science*, 3(4), 268–274.

Souami, D., & Souchay, J. (2012). The solar system's invariable plane. *Astronomy & Astrophysics*, 543, A133.

Veres, D., et al. (2013). The Antarctic ice core chronology (AICC2012). *Climate of the Past*, 9, 1733–1748.

Vieira, L. E. A., Norton, A., Dudok de Wit, T., Kretzschmar, M., Schmidt, G. A., & Cheung, M. C. M. (2012). How the inclination of Earth's orbit affects incoming solar irradiance. *Geophysical Research Letters*, 39, L16104.

Vondrák, J., Capitaine, N., & Wallace, P. (2011). New precession expressions, valid for long time intervals. *Astronomy & Astrophysics*, 534, A22.